Applied Physics A (2020) 126:118
https://doi.org/10.1007/s00339-019-3275-4

Applied Physics A
Materials Science & Processing

Investigation on energy dissipation by polarization switching in ferroelectric materials and the feasibility of its application in sound wave absorption

Haoyuan Du[1] · Dan Wang[1] · Linxiang Wang[1] · Roderick Melnik[2]

Received: 11 October 2019 / Accepted: 31 December 2019 / Published online: 21 January 2020

Abstract
In the current paper, energy dissipation via stress-induced polarization switching in ferroelectric material is investigated, and the feasibility of its application in sound wave absorption is analysed**.** For the system design and analysis, a phenomenological model based on the modified Landau phase transition theory is constructed to describe the polarization switching. A simple and robust energy dissipation prototype is introduced. The hysteretic dynamics associated with the polarization switching process and the energy dissipation process are investigated. The dependence of the energy dissipation on the bias voltage, frequency, and resistance is analysed in detail. The energy dissipation density in one cycle is calculated. It is shown that the resistance has a strong influence on the energy dissipation. Meanwhile, a better energy dissipation effect could be obtained by setting an appropriate resistance for the low-frequency excitation. The feasibility of using ferroelectric materials for low-frequency sound wave absorption is validated. For a specific acoustic energy dissipation device, corresponding design and analysis will be discussed in our future papers.

Keywords Ferroelectric · Polarization switching · Acoustic energy dissipation · Low frequency · Feasibility

1 Introduction

Attenuation or absorption of harmful noise is a commonly investigated topic, because there is always a need to mitigate the harmful effects that noise may have on human health. It is always desirable, often urgent, to find an effective way to absorb harmful noise or at least attenuate it to some extent. However, this is still a difficult challenge, particularly for the absorption of low-frequency sound waves. The strategies for sound wave absorption can be roughly classified into two approaches. One is the active sound wave absorption method. Using the inverse piezoelectric effect, active sound absorption can be achieved by actively adjusting the acoustic impedance of the composite sound-absorbing structure, and an anti-phase sound wave can also be actively emitted to produce active sound attenuation. Many efforts have been devoted to active sound wave attenuation and absorption [1–3]. A panel that could provide proper reflection coefficients with electrical control was designed to actively block sound wave propagation by Zhu et al. [1]. A wave separation algorithm was used to improve the control system of that panel. Using that algorithm, real-time control of acoustic transmission was achieved in the experiment. That panel was also proved to have a substantial effect on blocking broadband acoustic transmission. Moreover, a thin and light active underwater large-scale acoustic structure was developed by Wang et al. [2], which could satisfy the particular requirements of underwater application. Moreover, a shunt damping multi-layered piezoelectric coating with semi-active control for broadband echo reduction was also researched [3]. The active sound-absorbing technology does have an excellent sound-absorbing effect, even for low-frequency sound waves, but it requires a real-time measurement of sound pressure and phase on the sound wave propagation path and accurate real-time drive control of the piezoelectric structure. It is still difficult to achieve

✉ Linxiang Wang
wanglx236@zju.edu.cn

[1] State Key Laboratory of Fluid Power and Mechatronic Systems, Zhejiang University, 310027 Hangzhou, People's Republic of China

[2] MS2Dicovery Interdisciplinary Research Institute, Wilfrid Laurier University, Waterloo, ON N2L 3L5, Canada

large-scale applications for the complex system structure because of the low reliability and enormous input energy [4].

The other method is the passive acoustic absorption method, which is the continuous conversion of vibrational energy into other forms of energy without the addition of additional energy. Conventional passive acoustic absorption technologies are often based on viscoelastic materials [5, 6] and the mechanism of wave energy dissipation is to transform the vibration energy into thermal energy using the intrinsic viscoelastic damping of the material [5]. However, the absorption effect of the sound wave is proportional to the frequency of sound waves. For low-frequency sound wave absorption, the limitation of this technique is obvious, because the energy dissipation in each period via damping effects is still limited, and the number of repeated energy dissipation effects is also small in the same given period compared with those of medium- and high-frequency waves [7, 8]. Another passive sound wave absorption technology is the use of the electromechanical coupling effect of piezoelectric materials to convert vibration energy into electric energy and thermal energy automatically, which is very convenient for passive sound absorption, because a sound wave is a type of vibration essentially. A piezoelectric shunt damping technique based on the inherent mechanic-electric coupling effect of piezoelectric materials has been widely used in the field of both passive and active sound and vibration control fields [9–13]. Due to its promising application potential, the piezoelectric shunt damping technology has become a more and more attractive research topic and has been applied in various applications [4, 14, 15].

The essence of passive sound wave absorption and vibration attenuation is energy dissipation. In the conventional form, the vibration energy is first converted into electric energy and then converted into thermal energy via electrical resistance. The energy converted from the mechanical form directly to the thermal form is so small that it is usually neglected. The energy dissipation efficiency is affected profoundly by the following limitations. One limitation is that the produced strain amplitude is approximated proportional to the applied stress (imping wave pressure) and is rather small, according to the piezoelectric effects. The second limitation is also associated with the approximated linearity between the strain and applied stress. In piezoelectric effects, the produced strain is synchronized with the applied stress. One of the consequences of the synchronization is that, when the applied stress returns to zero, the energy dissipated that has not been dissipated will be re-converted into vibration energy, which requires a high demand for shunt damper circuits. To enhance the energy dissipation, there are various active switching circuits and control strategies were proposed, to break the synchronization between the produced voltage and the applied stress [16–18].

To overcome the mentioned limitations caused by the energy conversion mechanism based on piezoelectric effects, one candidate approach is stimulated using stress-induced polarization switching in ferroelectric or ferromagnetic materials to enhance the mechanical energy dissipations, because stress-induced polarization switching has a powerful damping effect on the mechanical excitations [19–20].

For ferromagnetic materials, the use of phase transition to promote energy dissipation was reported in Ref.[21]. In the investigation, a low-frequency mechanical load of 10 Hz was used to induce magnetization orientation switching in $Ni_{51.1}Mn_{24}Ga_{24.9}$ single crystals (ferromagnetic material) and power outputs of a few milliwatts were obtained without any parameter optimization. The enhancement of energy dissipation via mechanically induced magnetization orientation switching was reported in Ref.[22]. The magnetic shape memory alloy specimen was under a strain loading between 2 and 6%, with a frequency from 1 to 20 Hz. Two models were proposed to calculate the output voltage produced by the magnetization orientation switching, and both models could closely predict the voltage compared with the experimental results. In Ref.[23], acoustic energy harvesting using a Helmholtz resonator via magnetic shape memory alloys was researched, and the governing equations were obtained. The effect of different factors in the proposed energy harvester on the power generated was researched by solving the equations numerically.

For ferroelectric materials, it was illustrated experimentally that there would be 90° reversible polarization switching induced in $BaTiO_3$(ferroelectric materials) and $Pb(Mn_{1/3}Nb_{2/3})O_3 - PbTiO_3$(0.62PMN − 0.38PT) (ferroelectric materials) by electro-mechanic coupling loads. Considerable strain and voltage were obtained [24]. In $Pb(In_{1/2}Nb_{1/2})O_3 - Pb(Mg_{1/3}Nb_{2/3})O_3 - PbTiO_3$(PIN−PMN−PT) ferroelectric crystals, the energy dissipation was also experimentally studied by measuring the output voltages with different periodic applied stresses [25]. It was shown that the output power was significantly larger than that in linear piezoelectric materials in both open and closed circuits. Theoretic investigations on the polarization switching in ferroelectric materials induced by stress were also performed [26–28]. It was found that the applied stress could cause 90° polarization switching in the poled ferroelectric materials, and the polarization switching had a very strong damping effect on mechanical excitations [26, 27]. Based on the same mechanism, a strategy was proposed to use the stress-induced polarization switching to harvest vibration energy, and numerical simulations of the microstructure change were presented [28]. It was found that the robustness of the vibration energy harvester could be improved using a bias electric field. Moreover, the influence of the mechanical boundary conditions, resistance, and other factors on the energy harvester were analysed using the phase-field method. Dong et al. researched the effects of

load resistance and frequency on energy dissipation using the mechanically excited phase transformation in PIN−PMN−PT single crystal experimentally and a max mechanical energy dissipation value of 1.90 kJ m^{-3} $cycle^{-1}$ [29] was obtained. In composite materials consisting of ferromagnetic and ferroelectric compounds, amplified switching caused by both magnetic and dielectric subsystems can be observed [30, 31]. Moreover, there are promising dielectric materials for practical use, such as complex iron oxides [32, 33]. The main advantage of these materials is the stability of the chemical composition in air when heated up to 1000 K. Large spontaneous dielectric polarization and multiferroic properties at room temperature are recently discovered in barium hexaferrites substituted by diamagnetic cations [34, 35]. Existence of spontaneous polarization will facilitate polarization switching. Moreover, hexaferrites are not only dielectrics, but also magnetodielectrics with very strong magnetic properties, which are well worth considering [36, 37]. The existence of spontaneous magnetization will facilitate induced magnetization switching.

In the current paper, energy dissipation using the stress-induced polarization switching in ferroelectric material is investigated. A modified phenomenological model based on the Landau phase transition theory is constructed to model the polarization switching in ferroelectric materials induced by stress. A simple and robust energy dissipation prototype is used. The dependence of the bias voltage, frequency, and resistance on energy dissipation is systematically analysed in detail. The proposed prototype can adapt to the target frequency range better by changing the applied voltage and resistance. Moreover, the dissipated power density as a function of frequency is plotted. It is noted that the method of amplifying sound waves or vibration and how it can be used to induce the polarization switching will be presented in our future papers.

2 Energy dissipation mechanism

2.1 Prototype of the energy dissipation

Piezoelectric and ferroelectric materials consist of domains. Each domain has one polarization orientation. The essence of the current proposal for energy dissipation is to induce polarization switching in ferroelectric materials when the stress wave impinges on a properly designed composite structure with a ferroelectric element embedded. When polarization switching is induced by the stress applied in ferroelectric materials, voltage changes will be created at both sides of the material. Through a specially designed external shunt damping circuit (including resistance), the electric energy will be converted into heat energy to achieve the purpose of energy dissipation. The advantages of dissipating energy with ferroelectric material will be discussed in Sect. 2.2 in detail. The energy dissipation prototype adopted is similar to the traditional vibration energy dissipation devices [38]. The ferroelectric thin film is attached to a vibration amplification structure, such as a cantilever, which can enlarge the amplitude of the vibration. On both sides of the ferroelectric film are two electrodes connected to the dissipation circuit, as shown in Fig. 1a. The amplified stress is must larger than the coercive stress to induce the polarization switching. If not, only the linear piezoelectric effect works, which has a little effect on energy dissipation. When the ferroelectric film is subjected to compressive stress, the initially horizontal domains will be induced to switch perpendicularly. However, there are two possible variants, downward and upward, having equal chance, as shown in Fig. 1b. To have a better effect of the energy dissipation and energy conversion, a macroscopic polarization switching must be formed along the electrodes (perpendicular) direction, as shown in Fig. 1c [28]. Thus, a preference for the polarization switching must be given, and a bias electric field is supplied by a DC voltage source. With

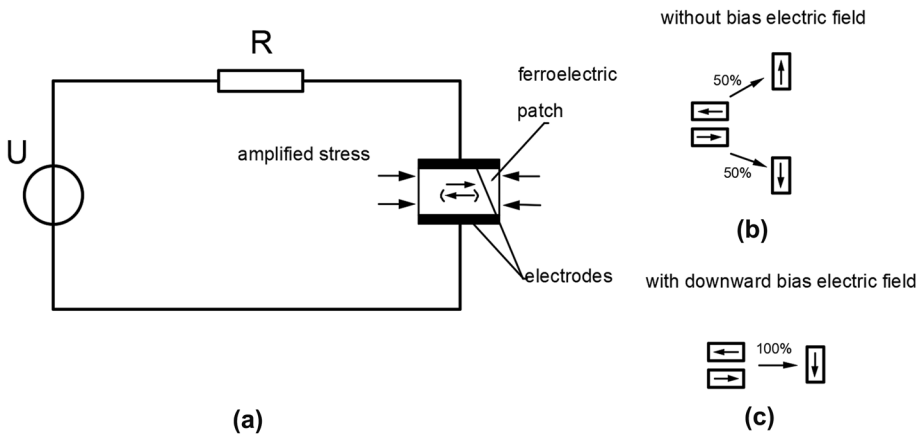

Fig. 1 The prototype of the energy dissipation

the bias electric field, only the downward direction will be chosen when the horizontal domains switch to the perpendicular direction, as shown in Fig. 1c. Moreover, as shown in Fig. 1a, a resistance is connected with the ferroelectric film in series to tune the energy dissipation effect.

It can be easily proved that, in a complete energy harvest cycle, the work done by the DC voltage can be calculated by [28]:

$$W_{\mathrm{DC}} = \int U_{\mathrm{DC}} I \mathrm{d}t = U_{\mathrm{DC}} \int I \mathrm{d}t = U_{\mathrm{DC}} \left(Q_{\mathrm{out}} - Q_{\mathrm{in}} \right). \quad (1)$$

In one complete cycle, Q_{out} equals Q_{in}, that is to say, the work done by the DC voltage source in one entire period is zero. The input mechanical energy is converted into two parts. One is converted into thermal energy in the process of polarization switching. The other is converted into electrical energy and dissipated by the resistance in the circuit.

2.2 Advantages of ferroelectric energy dissipation

The energy dissipation mechanism via 90° polarization switching induced by stress in ferroelectric materials is much more efficient than that in piezoelectric materials. The difference is illustrated clearly by Fig. 2. As shown in Fig. 2a, when external stress is applied to piezoelectric materials, there will only be a minor deviation of the polarization orientation, and no polarization switching is induced. The deviated orientation will be automatically restored once the external stress loading is removed. However, as for ferroelectric materials, when the external stress is larger than the coercive stress, as shown in Fig. 2b, 90° polarization switching will be induced. An attractive property of the stress-induced polarization switching is that, once the polarization switching is induced, a significant strain will be produced. At the same time, the domain will remain switched and will not be restored automatically to its original orientation. To restore its orientation, extra mechanical or electrical work is needed.

Obviously, from the energy conversion point of view, the polarization switching can be used for passive mechanical energy dissipation. When the stress provided by the system exceeds the coercive field of the ferroelectric material, the polarization switching can be induced. Using the strong damping effect of the polarization switching, the stress wave can be quickly absorbed and dissipated.

The advantages of using the stress-induced polarization switching in ferroelectric material for sound wave absorption and vibration attenuation can be explained as follows. As shown in Fig. 3, when the external stress is applied to the ferroelectric materials, the strain and output strain will exhibit strong nonlinearity, and hysteresis loops will occur in their relationships. The energy conversion will be significantly improved due to the following facts.

The first fact is that phase change heat will be created, and part of the vibration energy can be directly converted into the thermal form in the process of polarization switching. Second, the strain produced by the polarization switching is much larger than that in the linear piezoelectric effect. Finally, the produced strain is not synchronized with the applied stress, and a hysteresis loop is created [21]. Moreover, as shown in Fig. 3b, the value of strain is approximately swapped between two platforms, which means that the polarization switching is induced. In other words, the strain is leaping between two values, and the leaps take place with the same rhythm with the polarization switching. This fact can enhance the energy dissipation efficiency, because, when the polarization switching occurs, phase transition heat will be produced to promote the dissipation of vibration energy. Moreover, its working frequency bandwidth can be naturally

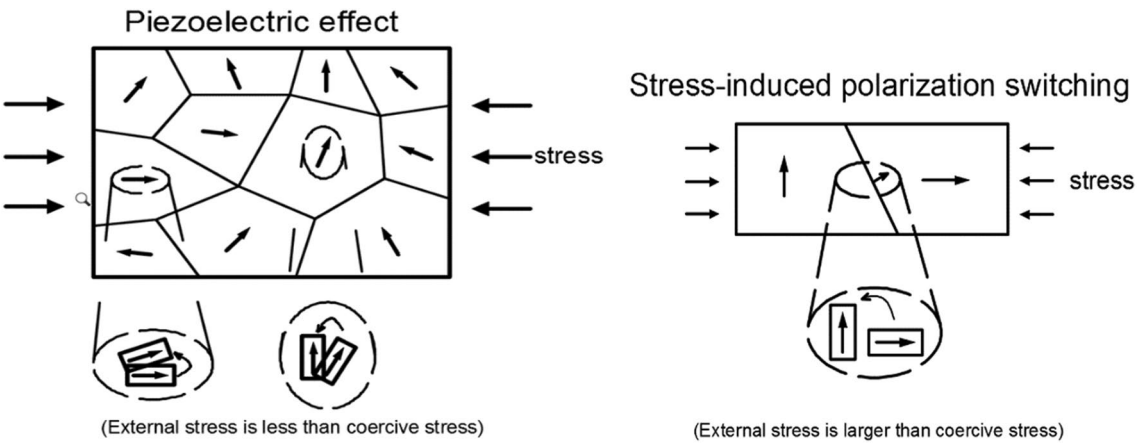

Fig. 2 The difference between the piezoelectric effect and stress-induced polarization switching. **a** Piezoelectric effect and **b** stress-induced polarization switching

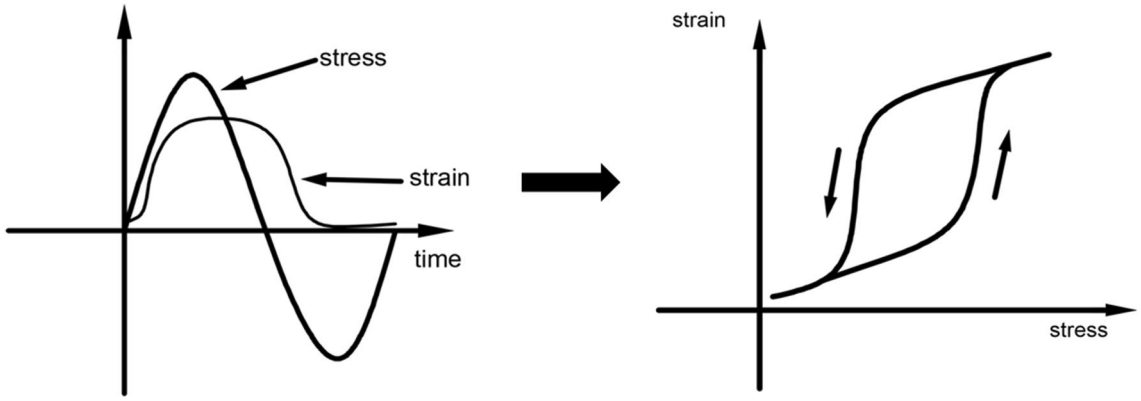

Fig. 3 The schematic diagram of the nonlinear force electric coupling relationship of a ferroelectric material

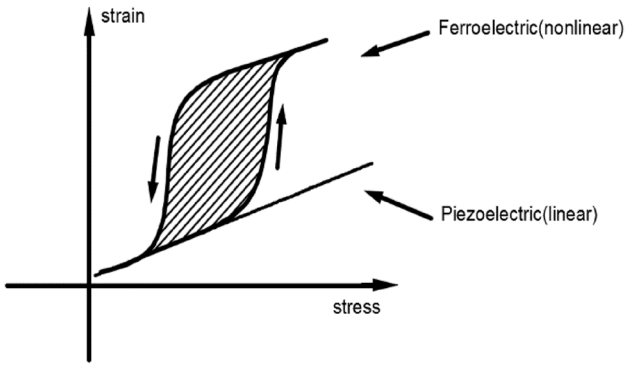

Fig. 4 Mechanical energy loss in polarization switching

broadened without using a deliberately designed synchronized switching shunt circuit [26, 27, 39].

To estimate the amount of energy dissipation, the typical stress–strain relations of the ferroelectric material and typical piezoelectric material are briefly outlined in Fig. 4. The hysteresis loop is due to the existence of the polarization switching. It is easy to see that the area of the hysteretic loop enclosed by the solid line (the shadow in the diagram) corresponds to the dissipated energy density of the input stress. In addition, there is no hysteresis loop in the linear piezoelectric effect. Thus, the energy dissipated by the linear piezoelectric effect can be ignored compared with that of the ferroelectric material.

2.3 Hysteretic dynamics and governing equations

For quantitative analysis of energy dissipation, the model constructed in Ref.[26] is employed and slightly modified here. For the modeling of polarization switching, the potential energy, kinetic energy, and dissipation energy are considered in the system, and the temperature is assumed to be below the Curie temperature. The polarization switching could be induced by electrical or mechanical loadings. The polarization orientations under the current investigation are taken as the cubic-tetragonal switching, which has three tetragonal and six orientations in the 3D system, as illustrated in Fig. 5a.

The three-dimensional switching can be simplified into a one-dimensional system as shown in Fig. 5b, and is still able to account for the hysteretic dynamics of the material [40, 41]. Figure 5c is the Landau free energy of the system, and each minimum value corresponds to the orientation in Fig. 5b. By simulating the switching between the horizontal

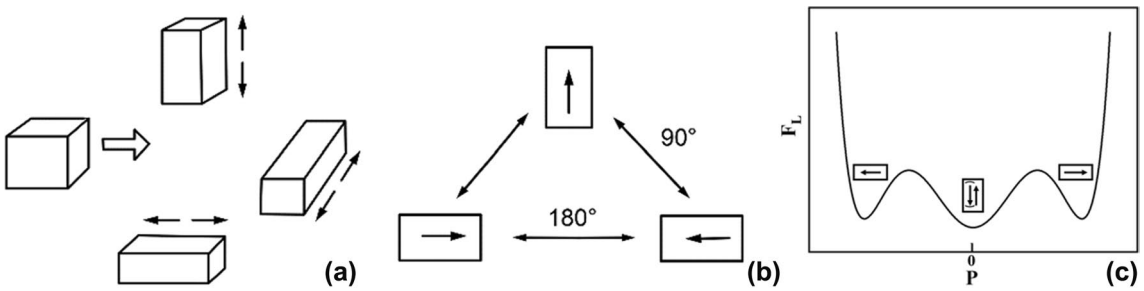

Fig. 5 Schematic of polarization switching in ferroelectric materials. **a** The six polarization orientations in the 3D system. **b** The three polarization orientations in the 1D system. **c** The Landau free energy having three local minima

and vertical rectangles in the one-dimensional system, the stress-induced 90° polarization switching can be incorporated [40–42].

Considering the energy contributions from the thermal, electric, and mechanical fields, the potential energy for the 1D analogue of polarization switching based on the Landau theory of phase transformations is constructed in the following form:

$$W(\theta, P, \varepsilon) = \varphi(\theta) + \frac{a_2}{2}P^2 + \frac{a_4}{4}P^4 + \frac{a_6}{6}P^6 + \frac{k}{2}\varepsilon^2 + \frac{b}{2}\varepsilon P^2, \tag{2}$$

where w, θ,ε, and P are the potential energy of the system, temperature, elastic strain, and polarization, respectively. $\varphi(\theta)$ is the energy in the thermal field, $\left(\frac{a_2}{2}P^2 + \frac{a_4}{4}P^4 + \frac{a_6}{6}P^6\right)$ is the energy in the electric field, $\left(\frac{k}{2}\varepsilon^2\right)$ is the energy in the mechanical field, and the $\left(\frac{b}{2}\varepsilon P^2\right)$ is the electromechanical term. Because the ferroelectric material is only used in the temperature below the Curie temperature and no thermal-induced polarization switching will be induced, the energy term in the thermal field $\varphi(\theta)$ can be ignored, and the potential energy can be simplified as:

$$W(P, \varepsilon) = \frac{a_2}{2}P^2 + \frac{a_4}{4}P^4 + \frac{a_6}{6}P^6 + \frac{k}{2}\varepsilon^2 + \frac{b}{2}\varepsilon P^2. \tag{3}$$

By choosing suitable coefficient values, the function can be tuned to handle the orientation switching [26]. Using Lagrange's equations, the motion of the system can be described. The kinetic energy of the proposed system is described by the following equation [26]:

$$U = \frac{1}{2}\left(I_{\mathrm{P}}\left(\frac{\mathrm{d}P}{\mathrm{d}t}\right)^2 + I_{\varepsilon}\left(\frac{\mathrm{d}\varepsilon}{\mathrm{d}t}\right)^2\right), \tag{4}$$

where I_{P} and I_{ε}, respectively, denote the material constants in the electric and mechanical field related to the generalized inertial effects in polarization switching.

To account for the dissipation effects of the switching process, a dissipation function is introduced as follows:

$$R = \frac{1}{2}\left(\tau_{\mathrm{P}}\left(\frac{\mathrm{d}P}{\mathrm{d}t}\right)^2 + \tau_{\varepsilon}\left(\frac{\mathrm{d}\varepsilon}{\mathrm{d}t}\right)^2\right), \tag{5}$$

where τ_P and τ_{ε} are material constants related to the friction part in polarization switching in the electric and mechanical fields, respectively.

The governing equations of the dynamics of the ferroelectric material under mechanical loadings (stress σ) and electric loadings (electric field E) can be formulated as the following two equations by employing the Euler–Lagrange equation with Eqs. 3–5 [26]. The generalized inertial effects can be ignored, because most experimental observations have proved that the inertial effects are much smaller than the damping effects [26]. Thus, the governing equations can be simplified by setting τ_P and I_{ε} equal to zero as follows:

$$\tau_{\mathrm{P}}\frac{\mathrm{d}P}{\mathrm{d}t} + a_2P + a_4P^3 + a_6P^5 + b\varepsilon P - E = 0, \tag{6a}$$

$$\tau_{\varepsilon}\frac{\mathrm{d}\varepsilon}{\mathrm{d}t} + k\varepsilon + \frac{bP^2}{2} - \sigma = 0. \tag{6b}$$

It can be seen that there are seven model parameters $(\tau_P, \tau_{\varepsilon}, a_2, a_4, a_6, b, k)$, which can be estimated using experimental data. The details of parameter estimation are given in Refs. [24] and [28]. It is demonstrated that the hysteresis loops in the stress-polarization and stress–strain curves can be successfully captured by the model given by Eq. (6).

2.4 Parameter dependence

For the convenience of numerical simulations, the values of the model parameters are taken from Refs. [26, 41], in which the model parameters are identified from the experimental data of $\mathrm{Pb}(\mathrm{Mg}_{1/3}\mathrm{Nb}_{2/3})\mathrm{O}_3 - \mathrm{PbTiO}_3 - \mathrm{BaTiO}_3$(PMN − PT − BT) in Ref. [43]. The amplified stress is assumed to be $\sigma = \sigma' \sin(2\pi ft)$, where σ' is the amplitude of the stress. The dimensionless material parameters are defined as:

$\tilde{\tau}_P = \tau_P/\tau_{P0}$, $\tilde{P} = P/P_0$, $\tilde{E} = E/E_0$, $\tilde{\varepsilon} = \varepsilon/\varepsilon_0$, $\tilde{a}_2 = aP_0/E_0$, $\tilde{a}_4 = a_4P_0^3/E_0$, $\tilde{a}_6 = a_6P_0^5/E_0$, $\tilde{\sigma} = \sigma\varepsilon_0/(P_0E_0)$, $\tilde{k} = k\varepsilon_0^2/(P_0E_0)$, $\tilde{b} = b\varepsilon_0P_0/E_0$, $\tilde{f} = f\tau_{P0}P_0/E_0$, $\tilde{t} = tE_0/(\tau_{P0}P_0)$, $\tilde{\tau}_{\varepsilon} = \tau_{\varepsilon}/\tau_{\varepsilon 0}$,where $P_0 = 10^{-2}$ c m^{-2}, $E_0 = 10^6$ V m^{-1}, $\varepsilon_0 = 1\%$, $\tau_{P0} = 10^6\Omega m$, and the dimensionless parameter used are taken as [26]:$\tilde{a}_2 = -1.06, \tilde{a}_4 = 51001.48.01, \tilde{a}_6 = -1797.95$, $\tilde{b} = -2580.16$, $\tilde{k} = 65.42$, $\tilde{\tau}_P = 0.01$, and $\tilde{\tau}_{\varepsilon} = 0$.

Moreover, an electrical equation is introduced in the proposed prototype as shown in Fig. 1a as follows:

$$U - \mathrm{RA}\frac{\mathrm{d}P}{\mathrm{d}t} - \mathrm{EL} = 0, \tag{7}$$

where U, R, A, and L are the values of the DC voltage source, resistance, area, and length of the ferroelectric materials, respectively. $A\frac{\mathrm{d}P}{\mathrm{d}t}$ is the current produced by the ferroelectric material [44]. The area is chosen as 10^{-4} m^2, and the length is 10^{-3} m.

Only the steady-state behaviour is considered here. The dependence of the applied voltage, the frequency of stress, and the resistance to the energy dissipation are analysed in the next sections.

2.5 Applied voltage dependence

In this part, the applied stress is chosen as a sinusoidal function $\tilde{\sigma} = -80\sin(2\pi t)$, where a negative value of the stress represents tensile stress. The voltage is applied at different

values, in particular, $U = 1$, 10, 50, 100, and 500 V. The dependence of the resistance will be analysed later in this article. Thus, R is set to be 0 in this part. The $\tilde{\sigma} - \tilde{P}$ curves of the simulated orientation switching are presented in Fig. 6.

It can be seen from Fig. 6 that polarization switching in ferroelectric material is induced when the voltage is not very strong (less than 100 V). When the voltage is too large, such as 500 V, the downwardbias electric field is so strong that the stress-induced switching is entirely suppressed. In addition, there is no hysteresis loop in $\tilde{\sigma} - \tilde{P}$ curves, as indicated by the dotted line curve in the plot. In that condition, larger tensile stress is needed to make downward polarization ($P > 0$) switch back to the horizontal state ($P = 0$). However, the stress cannot be so large that it exceeds the limit that the ferroelectric material can bear, which will cause damage to it. It is also a waste of energy to some extent.

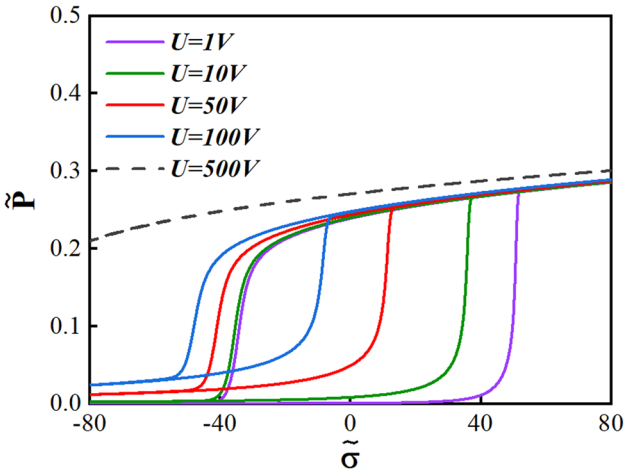

Fig. 6 The relationship of stress and polarization with different bias voltages

The simulated $\tilde{\sigma} - \tilde{\varepsilon}$ curves involving orientation switching with different voltages are presented in Fig. 7. It can be seen that the polarization switching has been successfully simulated using the model, and stress-induced polarization switching is a 90° switching, because the polarization values leap between 0 and a positive value. The polarization and strain both have strong hysteretic behaviour in their relationships with the applied stress caused by vibration. The mechanical energy density in one cycle can be calculated using numerical integration of the stress and strain data over one period:

$$W_{\text{mech}} = \int_0^{1/f} \sigma(t)\mathrm{d}\varepsilon(t). \tag{8}$$

It is obvious that W_{mech} is equal to the area of the stress–strain curve, as mentioned in Fig. 4. The larger the area is, the larger the amount of mechanical energy density dissipated in the polarization switching is. The dimensionless mechanical energy density ($\tilde{W}_{\text{mech}}$) in one cycle is calculated and shown in the upper left corner of each curve. Similar to the curves of $\tilde{\sigma} - \tilde{P}$, the shape of $\tilde{\sigma} - \tilde{\varepsilon}$ becomes 'thinner' and $\tilde{W}_{\text{mech}}$ in one cycle decreases as the applied

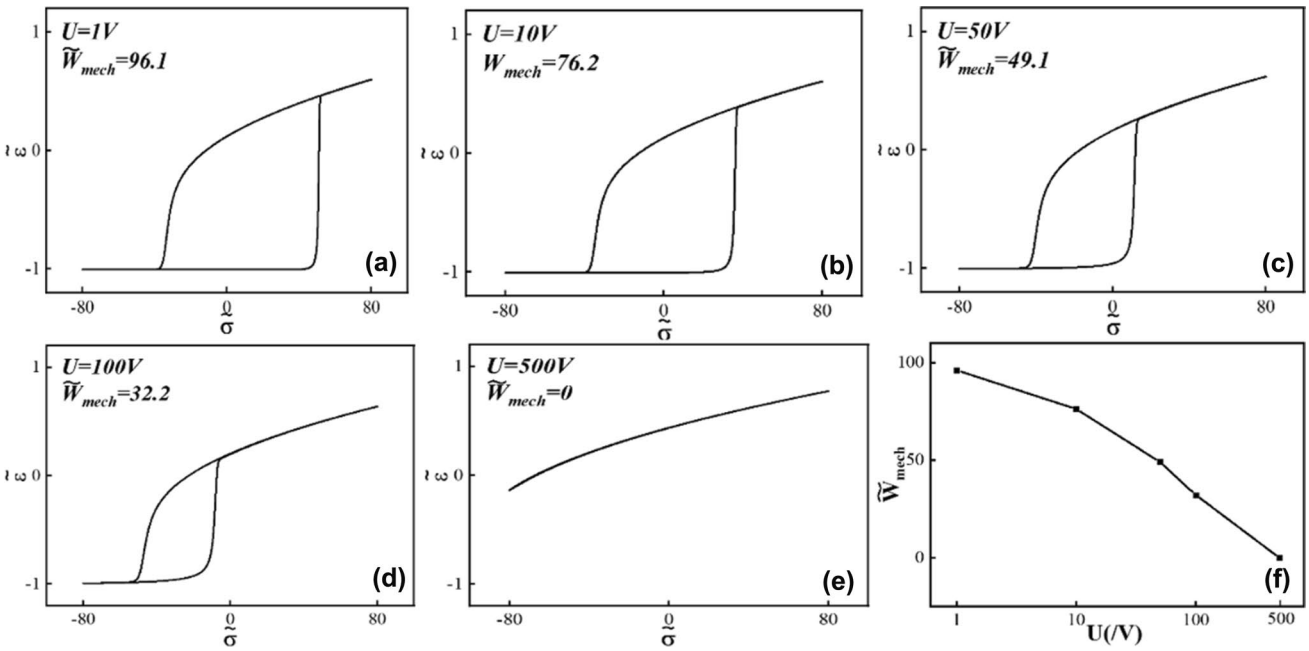

Fig. 7 The relationship of stress and stress with different bias voltages

voltage increases. The weaker the bias electric field strength is, the smaller the preference of the domain in the ferroelectric material is, and the larger the stress needed to cause the polarization switching is. Thus, more energy is required, and $\tilde{W}_{\text{mech}}$ is larger. When the electric field downward along the material is too large, the domain in the ferroelectric material is constrained in the perpendicular direction, and no polarization switching can be induced. Only the conventional mechanical–electric coupling effects contribute in energy dissipation, having a weak effect on energy dissipation.

By taking a closer look at the plots presented in Fig. 7, it is also interesting to mention the fact that the strength of the bias electric field has a massive influence on the stress-induced orientation switching. As plotted in Fig. 7a–c, the bias electric field is relatively weak, and horizontal to perpendicular polarization switching is induced by compressive stress, while the perpendicular to horizontal orientation switching is induced by tensile stress. For a stronger bias electric field, as sketched in Fig. 7d, both polarization switching types are induced by tensile stress. These observations can be explained by the coupling effects between the stress and electric fields, and the details of the mechanism will not be further discussed here, because it is outside the scope of this paper. As shown in Fig. 7e, the stress-induced polarization switching is completely suppressed when the voltage is strong enough, and no hysteresis loop exists. This fact means that the mechanical energy dissipation is very small, and only the conventional mechanical–electric coupling effects contribute in energy dissipation. The trend of the influence of voltage on energy dissipation is shown in Fig. 7f. It can be seen that, within the given range, the larger the voltage is, the smaller the energy dissipated in one cycle is.

2.6 Stress frequency dependence

It is known that the hysteresis of the ferroelectric material has a dependence on frequency. Thus, the energy dissipation using the ferroelectric is also influenced by the stress frequency. To analyse the effects of frequency on energy dissipation, the mechanical response of the ferroelectric material is investigated numerically here. The $\tilde{\sigma} - \tilde{\varepsilon}$ curves of the simulated polarization switching are presented in Fig. 8. The applied voltage (U) is fixed at 50V, the amplitude of the applied stress ($\tilde{\sigma}$) is chosen as 80. Moreover, the value of resistance is zero. The wave frequencies of $\tilde{\sigma}$ are selected from different values. For convenience, the dimensionless frequency $\tilde{f}$ and $\tilde{W}_{\text{mech}}$ is indicated in the $\tilde{\sigma} - \tilde{\varepsilon}$ curves in Fig. 8.

It is shown in Fig. 8 that the hysteresis loops in the stress–strain relationship change with $\tilde{f}$, and so does $\tilde{W}_{\text{mech}}$. This characteristic of the wave frequency dependence can be explained by the generalized inertial effects of the polarization switching process, which could be regarded as the effects of the time constants in Eq. (5). As also discussed in Ref.[29], the simulated hysteretic behaviour is a combination of the polarization switching and the response delay caused by a generalized inertial effect of the mechanical-electric response of the ferroelectric material. When the applied stress is at low frequency, the domain will have sufficient time to be reoriented. The delay due to the inertial effect can be neglected, because it is a minor contribution when the excitation is changing slowly. Therefore, the contribution to $\tilde{W}_{\text{mech}}$ is mainly from the polarization switching, as shown in Fig. 8a. When the frequency increases, the time for the domain to be reoriented becomes shorter, and its contribution to the loop area is decreased slightly. Meanwhile, the delay caused by the generalized inertial effects become more and more pronounced and have greater contribution to the loop area, as indicated by Fig. 8 a–d. At a specific frequency, the polarization switching contributing to the loop area is just cancelled by the increase to the loop area by the generalized effect, and the hysteresis loop will achieve its maximum area, as indicated in Fig. 8e. When the frequency increases even further, the contributions of the polarization reorientation that forms the hysteresis loop and the generalized inertial effect will both decrease, as indicated in Fig. 8g through (i). Meanwhile, $\tilde{W}_{\text{mech}}$ is becoming smaller and smaller.

To show the advantages of the polarization switching for energy dissipation, the temporal evolutions of the strain and produced current response are plotted as a time function in Fig. 9, together with applied stress at different wave frequencies. As the coordinate axes show, the black dotted line, solid blue line, and solid red line represent stress, strain, and the generated current, respectively. It is clearly shown that, when the frequency is relatively low, as in Fig. 9a, b, there are two leaps of the strain in one period, which means that polarization switching is induced. At the same time, the current exhibits a corresponding leap. The relatively even curve is the current caused by the linear piezoelectric effect, and it is easy to see that the current produced by the piezoelectric effect is quite smaller than that caused by polarization switching. Moreover, the shapes of the stress and strain are different, and there are phase lags, which are the causes of hysteresis loops. As mentioned earlier, the formation of hysteresis loops can dissipate a lot of energy. Thus, when the polarization switching is induced, more energy will be dissipated. When the frequency is increased, as in Fig. 9c, d, the strain has a similar shape to stress and no leap exists. Moreover, the amplitude of the strain is also much smaller, even though the magnitude of the applied stress is the same. This fact can be explained by the same mechanism as the competition between the domain reorientation and the generalized inertial effects. However, the amplitude of the produced current becomes even more extensive than that in

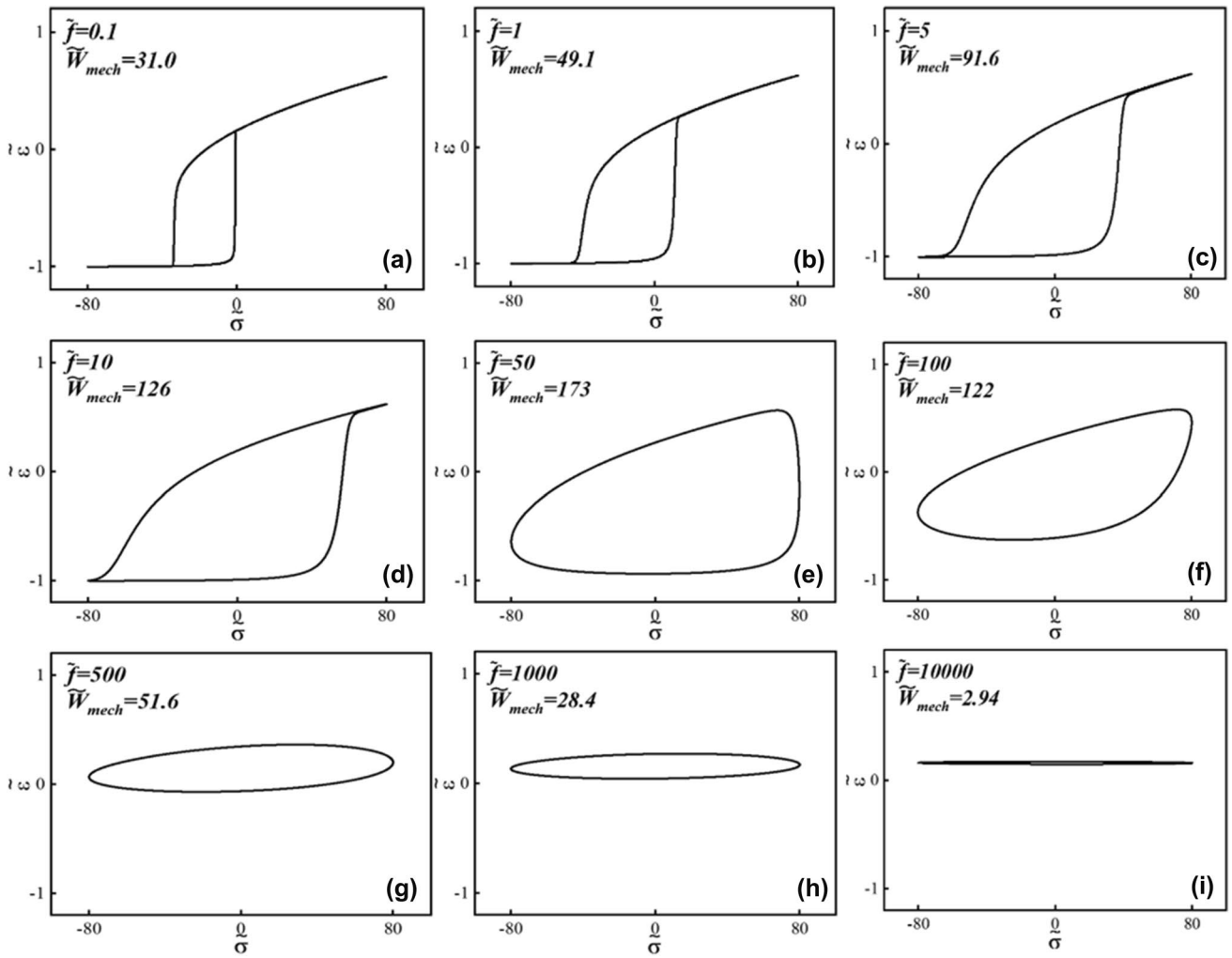

Fig. 8 Simulations of the effects of stress frequency on the strain

low frequency. This is because the current is caused by the change rate of the polarization [44], and although the value of polarization does not change much in high frequency, the high frequency makes the value of $\mathrm{d}P/\mathrm{d}t$ larger.

2.7 Resistance dependence

It is easy to know from the governing equations of this prototype that the resistance (R) in the circuit can influence the electric field applied to ferroelectric material and the current in the circuit. Small R means that most of U is applied on the ferroelectric material and a relatively large current, but the energy dissipated by R is related to the value of R and the magnitude of the current. Thus, it is necessary to research the dependence of R. For convenience of comparison, the stress is chosen as $\tilde{\sigma} = -80\sin(2\pi t)$, and $U = 1$, 10, 50, 100, and 500 V. Moreover, to have a comprehensive acknowledgement of the influence of the resistance, the values of the resistance are chosen as $R = 1$, 10^2, 10^4, $10^6$and 10^8 Ω, respectively.

The dependences of the resistance (R), dimensionless dissipated energy density ($\tilde{W}_{\mathrm{mech}}$), and electric energy ($\tilde{W}_{\mathrm{elec}}$) with different voltages are plotted in Fig. 10. The harvested electric energy can be calculated using [45]:

$$W_{\mathrm{elec}} = \int_0^{1/f} E(t)\mathrm{d}D(t), \tag{9}$$

where $E(t)$ is the electric field applied on the ferroelectric material and $D(t)$ is the electric displacement whose value can be adopted as the same as the polarization [44]. The values of $\tilde{f}$ are chosen as 1 and 100.

The relationships of the stress and strain when $U = 50$ V are plotted in Fig. 10a with different R. As can be seen, the hysteresis loop becomes fatter and fatter when R is no

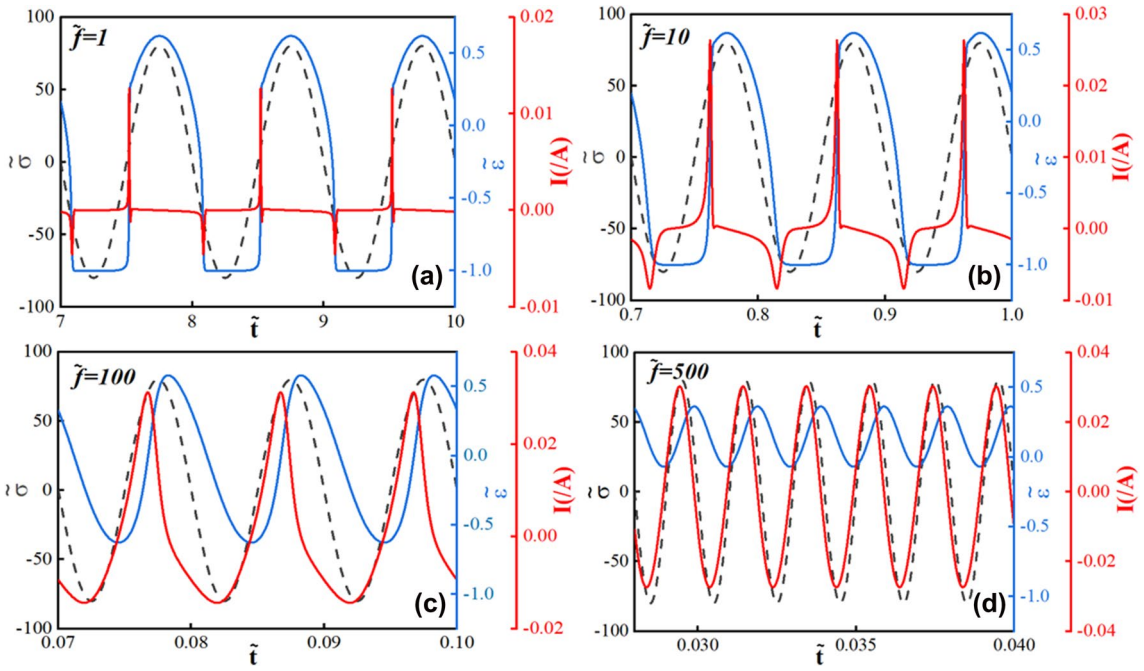

Fig. 9 The temporal evolution of stress, strain, and current in three periods

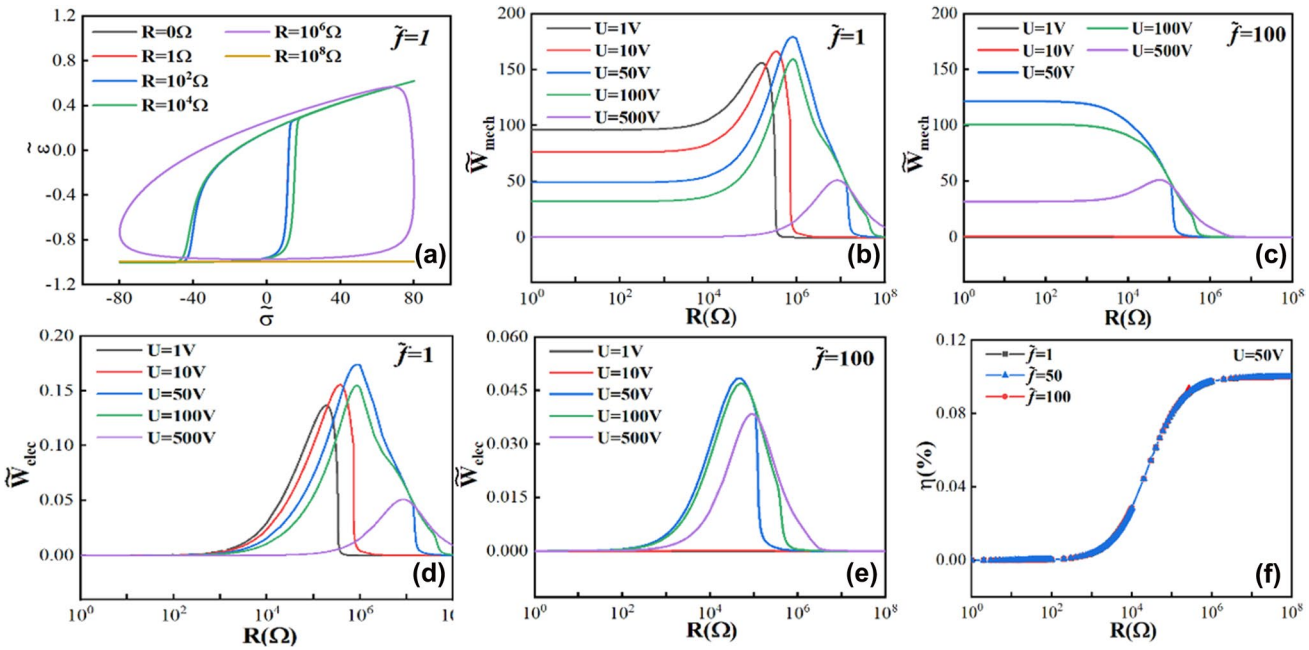

Fig. 10 The relationship of R and $\tilde{S}$ with different voltages

greater than 10^6 Ω.This is because, as R increases, the voltage applied to the ferroelectric decreases, which makes $\tilde{W}_{\mathrm{mech}}$ larger under these circumstances, as discussed in 4.1. Moreover, the larger the voltage on the R is, the more electrical energy can be dissipated. When R is as large as 10^8Ω, there is no hysteresis loop between $\tilde{\sigma}$ and $\tilde{\varepsilon}$, which is because the extremely large R makes the circuit nearly open, and there is no preference for polarization switching in the perpendicular direction.

In Fig. 10b, c, the $\tilde{W}_{\text{mech}}$ is plotted under the circumstances mentioned above with $\tilde{f} = 1$ and 100. As can be seen, when the value of R is less than 10^4 Ω, the $\tilde{W}_{\text{mech}}$ of the system nearly does not change at all under the applied voltages and given frequencies. Then, at the circumstances of $\tilde{f} = 1$, all of the curves are single peak, and the corresponding frequency of the peak increases with the increase of U. For an explanation, one can refer to the discussion in Fig. 10a, and the larger U is, the larger the R needed to reduce the voltage applied on the ferroelectric material to an optimal value is. When R is larger than the optimal value of the corresponding maximum $\tilde{W}_{\text{mech}}$, the curves with $U = 1\ V$ and $10\ V$, respectively, drop rapidly, because the voltage on the ferroelectric material is not large enough to provide the preference. Moreover, it is noticeable that $\tilde{W}_{\text{mech}}$ with $U = 500\ V$ is almost zero when the resistance is less than $10^6\Omega$. This is because, when R is not large, the voltage applied on the ferroelectric is still too large to induce the polarization switching, as mentioned before.

The trends of the dependence of R on $\tilde{W}_{\text{mech}}$ before the curve reaches its peak when $U = 1\ V$ and $10\ V$ are similar to the experimental data in Ref.[29]. This fact proves that the model used in this article is appropriate and can explain the empirical phenomena well. That is, the parameters in this model can be identified and adjusted according to the chosen material. Moreover, the behaviour of the ferroelectric material can be simulated and analysed further. The largest energy dissipated in this simulation is $177.60\ P_0E_0$ ($177.60\ \text{kJ m}^{-3}\text{cycle}^{-1}$) when $U = 50\ V$ and $R = 10^6\Omega$, which is larger than that in Ref.[29] ($1.90\ \text{kJ m}^{-3}\ \text{cycle}^{-1}$). The main reason is that the stress that induced the polarization in this simulation is larger.

However, when $\tilde{f}$ is 100, $\tilde{W}_{\text{mech}}$ becomes nearly 0 at all values of R when $U = 1\ V$ and $10\ V$. $\tilde{W}_{\text{mech}}$ with $U = 50\ V$ and $100\ V$ has platforms when R is less than $10^3\Omega$, and decreases rapidly when R is larger than $10^4\Omega$. This is because, when R is less than $10^3\Omega$, the U applied on the ferroelectric material does not change much, and higher frequency means stronger preference is needed. Thus, $U = 50\ V$ and $100\ V$, respectively, perform better than when $U = 1\ V$ and 10 V. However, $\tilde{W}_{\text{mech}}$ with $U = 500\ V$ reaches its maximum when R is approximately $10^5\Omega$. All of the values with R less than $10^6\Omega$ are more significant than that in $\tilde{f} = 1$ and decrease to zero when R becomes larger. The reason is similar to that mentioned above, and when $\tilde{f}$ is larger, the R corresponding to the peak is smaller. Thus, it can be concluded that, when the frequency is higher, stronger preference for the polarization switching is needed to have a larger $\tilde{W}_{\text{mech}}$.

For $\tilde{W}_{\text{elec}}$, all of the curves in Fig. 10d, e are also single-peak except when $U = 1\ V$ and $10\ V$ in Fig. 10e. The corresponding frequency of the peak increases with the increasing U, which is similar to $\tilde{W}_{\text{mech}}$ when $\tilde{f} = 1$.and When $\tilde{f} = 100$, the R corresponding to the peak is an order of magnitude smaller than that in $\tilde{f} = 1$. Moreover, $\tilde{W}_{\text{elec}}$ is almost zero when $U = 1\ V$ and $10\ V$.

The efficiency (η) of $\tilde{W}_{\text{mech}}$ to $\tilde{W}_{\text{elec}}$ is calculated in Fig. 10f at a U of $50\ V$ with $\tilde{f} = 1,\ 50,$ and 100. As can be seen, the η curves under three frequencies almost overlap entirely. There are two platforms when R is less than $10^3\Omega$ and larger than $10^6\Omega$, and η increases in these two intervals with increase of the R and reaches its maximum 0.1%. Although the value of η is not significant compared with other literatures [25, 29, 45, 46], the primary purpose of our prototype is to dissipate the mechanical energy as much as possible. Moreover, there is only a resistance without a particular harvested circuit for the consideration of robustness and simplicity. If it is needed, a harvested circuit can be attached, and much more energy can be harvested.

3 Energy dissipation dispersion

3.1 Energy dissipation density

To extend the analysis, $\tilde{W}_{\text{mech}}$ of the ferroelectric material with different voltages and resistances is considered as a function of frequency. The stress frequency $\tilde{f}$ is set in a range from 1 to 1000, and the amplitude of $\tilde{\sigma}$ is set as 80. The bias voltage is chosen as $U = 1$ V, 10 V, 50 V, and 100 V. The $\tilde{W}_{\text{mech}}$ with $R = 0\ \Omega$ in one cycle is calculated and plotted in Fig. 11a. For the convenience of analysis, the $\tilde{\sigma}$ axis is on a logarithmic scale. It is easy to identify the following facts. First, a single-peak curve is created by each U. This fact means that $\tilde{W}_{\text{mech}}$ decreases when $\tilde{f}$ is towards 1 or 1000, which is consistent with the discussion in Sect. 4.2. The peak value of each curve is the maximum $\tilde{W}_{\text{mech}}$ that could be achieved. The second is that the bias voltage U can influence the $\tilde{W}_{\text{mech}}$ effectively. When U is less than 50 V, larger U means that the $\tilde{f}$ corresponding to the maximum $\tilde{W}_{\text{mech}}$ is higher. U with the values of 1 V and 10 V is very sensitive to the frequency and only performs well in low frequency. When $\tilde{f}$ is larger than the corresponding value of the peak, $\tilde{W}_{\text{mech}}$ drops rapidly. When $U = 100$ V, the $\tilde{f}$ that makes the maximum $\tilde{W}_{\text{mech}}$ is the same as that in $U = 50$ V, but the maximum of $\tilde{W}_{\text{mech}}$ is smaller. Overall, $U = 50$ V has the best performance of energy dissipation and good adaptability to various frequencies when $R = 0\ \Omega$.

According to the discussion regarding the influence of resistance in Sect. 4.3, it is found that, when U is 1 or 10 V, no matter whether $\tilde{f}$ is 1 or 100, there is a small increase in $10^2\Omega$ and $10^4\Omega$. Thus, it is necessary to explore whether $\tilde{W}_{\text{mech}}$ will be more significant when $\tilde{f}$ is set to other values. $\tilde{W}_{\text{mech}}$ is plotted when $U = 1$ V and 10 V and the R = $10^2\Omega$

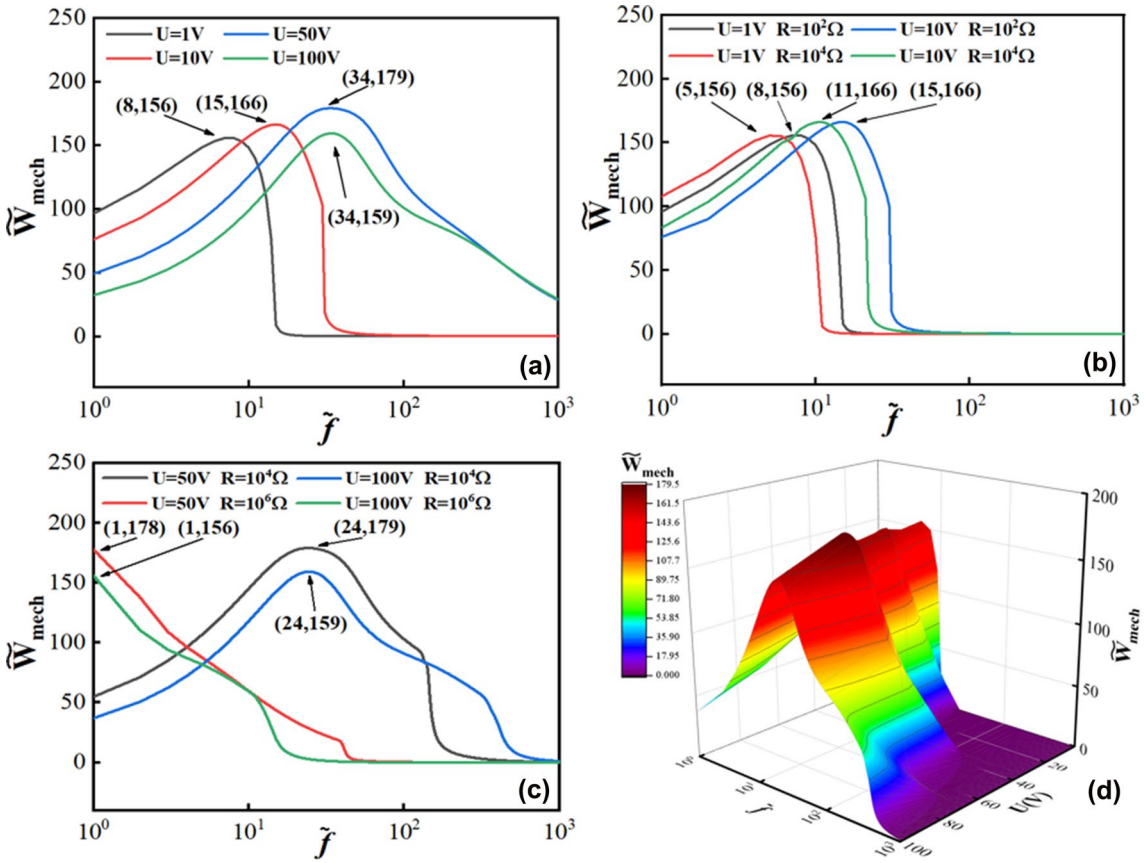

Fig. 11 $\tilde{W}_{mech}$ dispersion with different U and R as a function of $\tilde{f}$. **a** $R = 10^4\ \Omega$; **b**$U = 1$ V and 10 V, $R = 10^2\ \Omega$ and $10^4\ \Omega$, respectively; **c**$U = 50$ V and 100 V,R = $10^4\Omega and 10^6\Omega$, respectively; **d** 3D curve of the relationship of U, $\tilde{f}$, and $\tilde{W}_{mech}$ with $R = 10^4\ \Omega$

and $10^4\Omega$ respectively, in Fig. 11b. It is shown that the existence of R barely changes the shape of the curve in any circumstance. However, the increase of R leads to a leftward shift of the curve, and the $\tilde{f}$ corresponding to the maximum $\tilde{W}_{mech}$ decreases approximately 3–4 (300 − 400Hz) compared with those in $R = 10^2\Omega$ when the R is $10^4\Omega$.

Combined with the discussion regarding the influence of R, it is found that no matter whether $\tilde{f}$ is 1 or 100, when U is 50 or 100 V, the energy dissipation effect is better for $10^4\Omega$ and $10^6\Omega$. Therefore, $\tilde{W}_{mech}$ is analysed when $U = 50\ V$ and 100 V and $R = 10^4\Omega$ and $10^6\Omega$, respectively. The curves of $\tilde{f} - \tilde{W}_{mech}$ are plotted in Fig. 11c, and it is found that the shapes of the curves do not change much with $R = 10^4\Omega$; only the $\tilde{f}$ corresponding to the maximum $\tilde{W}_{mech}$ is 10 less than that in Fig. 10a. When R is $10^6\Omega$, the shapes of the curves change a lot and becomes a downward line. The lower $\tilde{f}$ is, the larger $\tilde{W}_{mech}$ becomes. Within the given range, the maximum $\tilde{W}_{mech}$ occurs when $\tilde{f}$ (100 Hz). Therefore, as can be seen, the main effect of R is to adjust the frequency range of the optimal dissipated energy of the system. When the target frequency is low, better dissipation effect can be obtained by increasing the R value to achieve the purpose of low-frequency energy dissipation. Therefore, it is feasible to use ferroelectric materials for low-frequency sound wave absorption.

To analyse the influence of $\tilde{f}$ and U on dissipated energy more comprehensively, combined with the above discussion, it is found that, when R is $10^4\Omega$, it can effectively reduce the optimal frequency range of the energy dissipation effect. Therefore, the three-dimensional diagram of dissipated energy with $R = 10^4\Omega$, $U = 1 - 100V$, and $\tilde{f} = 1 - 1000$ is plotted in Fig. 11d. It is seen that the voltage with the value of 50 V has the best effect of energy dissipation, because it can dissipate energy effectively on a large scale and $\tilde{W}_{mech}$ decreases slower than other voltages.

3.2 Power dissipation density

To obtain a better analysis of the dissipation ability of the ferroelectric material and make a foundation for research on energy conversion in the future, the mechanical power dissipation density (P_{mech}) is introduced to account for the total energy dissipation density in 1 s as follows:

$$P_{\text{mech}} = f \cdot W_{\text{mech}}. \tag{10}$$

Combined with the discussion in Sect. 5.1, $\tilde{P}_{\text{mech}}$ is plotted in Fig. 12 with different voltages and resistances as a function of frequency. The stress frequency $\tilde{f}$ is set in a range from 1 to 1000, the amplitude of $\tilde{\sigma}$ is set as 80, and the bias voltage is chosen the same as in Sect. 5.1 at $U = 1$ V, 10 V, 50 V, and $100V$, respectively. $\tilde{P}_{\text{mech}}$ dispersion with different U and R is a function of $\tilde{f}$. The shapes of the curves in Fig. 12 are different from those in Fig. 11. First, the $\tilde{P}_{\text{mech}}$ with $R = 0\ \Omega$ in one cycle is calculated and plotted in Fig. 12a, and for the convenience of analysis, the $\tilde{\sigma}$ axis is on a logarithmic scale.

The curves of $U = 1$ V, 10 V, and 50 V are still single peak, but the frequency corresponding to the peak is larger than those in Fig. 11a. The peak frequency increases as U increases. This is because, for the $\tilde{f}$ that is higher than the peak-corresponding frequency in Fig. 11, the $\tilde{W}_{\text{mech}}$ in one cycle may not be that large, but the number of periods in 1 s is larger when $\tilde{f}$ is higher, and $\tilde{P}_{\text{mech}}$ is the product of $\tilde{f}$ and $\tilde{W}_{\text{mech}}$. However, the curve $U = 100$ V is a growing curve in the given range. $\tilde{P}_{\text{mech}}$ increases with $\tilde{f}$, and it is reasonable to conclude that it is also a single-peak curve, but the peak frequency is out of range.

For the convenience of comparison, $\tilde{P}_{\text{mech}}$ is plotted when $U = 1$ V and 10 V and $R = 10^2\ \Omega$ and $10^4\ \Omega$ in Fig. 12b, respectively. As shown in Fig. 12b, the four curves have similar shapes, and the curves with $U = 10$ V perform better, which means that the U applied on the ferroelectric material is not sufficient. Larger R makes the U applied even smaller. $U = 10$ V and $R = 10^2\ \Omega$ has the best effect of $\tilde{P}_{\text{mech}}$.

Then, $\tilde{P}_{\text{mech}}$ is analysed when $U = 50$ Vand 100 V and $R = 10^4\Omega$and $10^6\Omega$, respectively, in Fig. 12c. The four curves are still single peak, and when the $R = 10^4\Omega$, $\tilde{P}_{\text{mech}}$ is more significant for both circumstances, especially in high frequency. This is mainly because, as shown in Fig. 11c, when $R = 10^6\Omega$, $\tilde{W}_{\text{mech}}$ only performs well in low frequency and decreases to nearly zero before $\tilde{f}$ reaches 100. Moreover, according to Eq. 10, $\tilde{P}_{\text{mech}}$ trends to zero, even though $\tilde{f}$ increases. $U = 100$ V and $R = 10^4\ \Omega$ has a better effect of $\tilde{P}_{\text{mech}}$, especially when $\tilde{f}$ is high, and this is because, as discussed in Sect. 4.3, higher frequency requires a larger voltage to provide stronger preference. According to Eq. 10 and Fig. 11c, a larger $\tilde{P}_{\text{mech}}$ is obtained when $U = 100$ V.

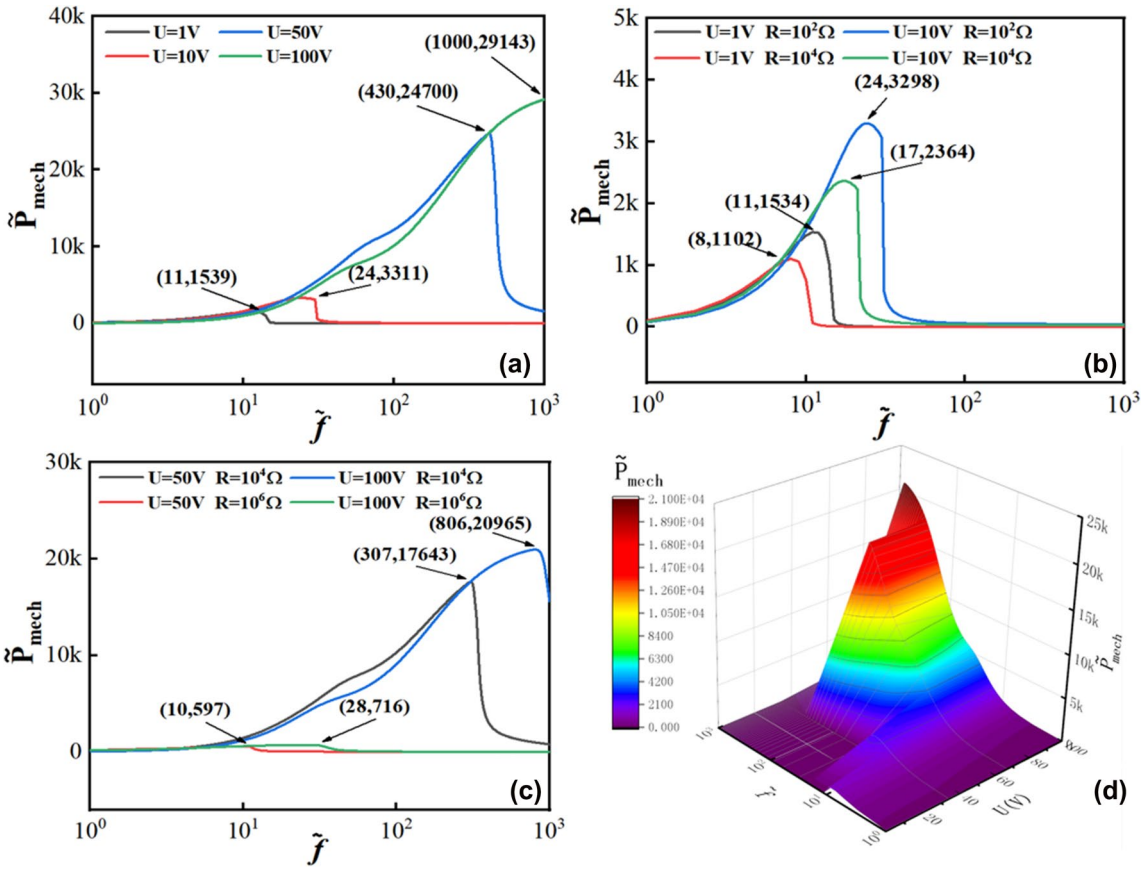

Fig. 12 $\tilde{P}_{\text{mech}}$ dispersion with different U and R as a function of $\tilde{f}$. **a** $R = 10^4\ \Omega$; **b** $U = 1$ V and 10 V, $R = 10^2\ \Omega$ and $10^4\ \Omega$, respectively; **c** $U = 50$ V and 100 V, $R = 10^4\ \Omega$ *and* $10^6\ \Omega$, respectively; **d** 3D curve of the relationship of U, $\tilde{f}$, and $\tilde{P}_{\text{mech}}$ with $R = 10^4\ \Omega$

Moreover, the influence of $\tilde{f}$ and U on $\tilde{P}_{\text{mech}}$ with $R = 10^4\Omega$ is plotted in Fig. 12d. As can be seen, large values of $\tilde{P}_{\text{mech}}$ in the graph are all concentrated in one corner with high voltage and frequency. It is noted that $U = 100V$ has the best effect of power dissipation, and referring to Fig. 12c, the largest $\tilde{P}_{\text{mech}}$ is obtained when $\tilde{f} = 806$. As mentioned before, this is mainly because $\tilde{P}_{\text{mech}}$ is the product of $\tilde{f}$ and $\tilde{W}_{\text{mech}}$, and when the difference of $\tilde{W}_{\text{mech}}$ is small, the increase in frequency is very important.

4 Conclusion

In the current paper, 90° polarization switching induced by stress in ferroelectric material and energy dissipation are researched. The feasibility of low-frequency sound wave absorption using ferroelectric materials is discussed. A phenomenological model based on the modified Landau phase transition theory is constructed to describe the polarization switching. A simple and robust energy dissipation prototype is used by introducing a preference for the polarization switching. The dependence of the parameters is investigated in detail. It is found that the bias voltage and the frequency have strong dependence on the stress-induced polarization switching and the energy dissipation. When the bias voltage and frequency are fixed, the largest energy dissipation density can be realized by changing the value of resistance. Moreover, the energy dissipation density dispersion curves are plotted, and it is found that the main effect of resistance is to adjust the frequency range of the optimal dissipated energy of the system. When the target frequency is low, a better dissipation effect can be obtained by increasing the resistance to achieve the purpose of low-frequency energy dissipation. Thus, it is feasible to use ferroelectric materials for low-frequency sound wave absorption. Finally, power dissipation density dispersion curves are plotted and discussed.

Acknowledgements This work was supported by the National Natural Science Foundation of China (Grant No. 51575478 and Grant No. 61571007).

References

1. H. Zhu, R. Rajamani, K.A. Stelson, Active control of acoustic reflection, absorption, and transmission using thin panel speakers. J Acoust Soc Am **113**(2), 852–870 (2003)
2. W. Wang, P.J. Thomas, Low-frequency active noise control of an underwater large-scale structure with distributed giant magnetostrictive actuators. Sens Actuators, A **263**, 113–121 (2017)
3. Y. Sun, Z. Li, A. Huang et al., Semi-active control of piezoelectric coating's underwater sound absorption by combining design of the shunt impedances. J Sound Vib **355**, 19–38 (2015)
4. H. Lissek, R. Boulandet, R. Fleury, Electroacoustic absorbers: bridging the gap between shunt loudspeakers and active sound absorption. J Acoust Soc Am **129**(5), 2968–2978 (2011)
5. Darabi B. Dissipation of vibration energy using viscoelastic granular materials. University of Sheffield, 2013.
6. G.C. Gaunaurd, High-frequency acoustic scattering from submerged cylindrical shells coated with viscoelastic absorbing layers. J Acoust Soc Am **62**(3), 503–512 (1977)
7. H. Zhao, J. Wen, D. Yu et al., Low-frequency acoustic absorption of localized resonances: Experiment and theory. J Appl Phys **107**(2), 1734 (2010)
8. Lin-Mei L, Ji-Hong W, Hong-Gang Z, et al. Low-frequency acoustic absorption of viscoelastic coating with various shapes of scatterers. ACTA PHYSICA SINICA, 2012, 61(21).
9. Z. Zhang, S. Li, Q. Huang, Low-frequency sound radiation of infinite orthogonally rib-stiffened sandwich structure with periodic subwavelength arrays of shunted piezoelectric patches. Compos Struct **187**, 144–156 (2018)
10. N. Jiménez, W. Huang, V. Romerogarcía et al., Ultra-thin metamaterial for perfect and quasi-omnidirectional sound absorption. Appl Phys Lett **109**(12), 455–157 (2016)
11. X. Li, Y. Chen, G. Hu et al., A self-adaptive metamaterial beam with digitally controlled resonators for subwavelength broadband flexural wave attenuation. Smart Mater Struct **27**(4), 045015 (2018)
12. Gardonio P, Casagrande D. Shunted piezoelectric patch vibration absorber on two-dimensional thin structures: Tuning considerations. J Sound Vib 2017, 395(Complete):26–47.
13. S. Manzoni, S. Moschini, M. Redaelli et al., Vibration attenuation by means of piezoelectric transducer shunted to synthetic negative capacitance. J Sound Vib **331**(21), 4644–4657 (2012)
14. R.L. Forward, Electronic damping of vibrations in optical structures. Appl Opt **18**(5), 690–697 (1979)
15. N.W. Hagood, A.V. Flotow, Damping of structural vibrations with piezoelectric materials and passive electrical networks. J Sound Vib **146**(2), 243–268 (1991)
16. A. Erturk, D.J. Inman, Broadband piezoelectric power generation on high-energy orbits of the bistable Duffing oscillator with electromechanical coupling. J Sound Vib **330**(10), 2339–2353 (2011)
17. H. Wu, L. Tang, Y. Yang et al., Development of a broadband nonlinear two-degree-of-freedom piezoelectric energy harvester. J Intell Mater Syst Struct **25**(14), 1875–1889 (2014)
18. J. Cheng, Semi-active vibration suppression by a novel synchronized switch circuit with negative capacitance. Int J Appl Electromagnet Mech **37**(4), 291–308 (2011)
19. M. Rezaeisaray, M. El Gowini, D. Sameoto et al., Wide-bandwidth piezoelectric energy harvester with polymeric structure. J Micromech Microeng **25**(1), 015018 (2014)
20. J. Li, X. Zhou, G. Huang et al., Acoustic metamaterials capable of both sound insulation and energy harvesting. Smart Mater Struct **25**(4), 045013 (2016)
21. I. Karaman, B. Basaran, H.E. Karaca et al., Energy harvesting using martensite variant reorientation mechanism in a NiMnGa magnetic shape memory alloy. Appl Phys Lett **90**(17), 1966 (2007)
22. N.M. Bruno, C. Ciocanel, H.P. Feigenbaum et al., A theoretical and experimental investigation of power harvesting using the NiMnGa martensite reorientation mechanism. Smart Mater Struct **21**(9), 299–312 (2012)
23. Farsangi M A A, Zohoor H. Acoustic energy harvesting via magnetic shape memory alloys. Journal of Physics D: Applied Physics, 2019, vol. 52(13), pp. 135501.
24. Y.W. Li, F.X. Li, Ultrahigh actuation strains in and single crystals via reversible electromechanical polarization switching. Appl Phys Lett **102**(15), 3408–1811 (2013)

25. W.D. Dong, J.A. Gallagher, C.S. Lynch, Ideal energy harvesting cycle using a phase transformation in ferroelectric crystals. Smart Mater Struct **23**(23), 125026 (2014)
26. L. Wang, R. Melnik, F. Lv, Stress induced polarization switching and coupled hysteretic dynamics in ferroelectric materials. Frontiers of Mechanical Engineering **6**(3), 287 (2011)
27. L.X. Wang, R. Liu, R.V.N. Melnik, Modeling large reversible electric-field-induced strain in ferroelectric materials using 90° orientation switching. Chinese Science: Technical Science **52**(4), 141–147 (2010)
28. Wang D, Wang L, Melnik R. Vibration energy harvesting based on stress-induced polarization switching: A phase field approach. Smart Materials & Structures, 2017, 26(6).
29. W.D. Dong, P. Finkel, A. Amin et al., Energy harvesting using the FER–FEO phase transformation in [011] cut single crystal PIN-PMN-PT. J Intell Mater Syst Struct **25**(14), 1786–1799 (2014)
30. S.V. Trukhanov, A.V. Trukhanov, M.M. Salem et al., Preparation and investigation of structure, magnetic and dielectric properties of bicomponent ceramics. Ceram Int **44**(17), 21295–21302 (2018)
31. M.M. Salem, L.V. Panina, E.L. Trukhanova et al., *Structural, electric and magnetic properties of composites* (Engineering, Composites Part B, 2019), p. 107054
32. A.V. Trukhanov, V.G. Kostishyn, L.V. Panina et al., Magnetic properties and Mössbauer study of gallium doped M-type barium hexaferrites. Ceram Int **43**(15), 12822–12827 (2017)
33. A.V. Trukhanov, S.V. Trukhanov, V.G. Kostishyn et al., Correlation of the atomic structure, magnetic properties and microwave characteristics in substituted hexagonal ferrites. J Magn Magn Mater **462**, 127–135 (2018)
34. Trukhanov S V, Trukhanov A V, Kostishin V G, et al. Coexistence of spontaneous polarization and magnetization in substituted M-type hexaferrites BaFe 12–x Al x O 19 (x⩽ 1.2) at room temperature. JETP letters, 2016, 103(2): 100–105.
35. A. Trukhanov, L. Panina, S. Trukhanov et al., Evolution of structure and physical properties in Al-substituted Ba-hexaferrites. Chin Phys B **25**(1), 016102 (2015)
36. S.V. Trukhanov, A.V. Trukhanov, L.V. Panina et al., Temperature evolution of the structure parameters and exchange interactions in. J Magn Magn Mater **466**, 393–405 (2018)
37. A.V. Trukhanov, M.A. Almessiere, A. Baykal et al., Influence of the charge ordering and quantum effects in heterovalent substituted hexaferrites on their microwave characteristics. J Alloy Compd **788**, 1193–1202 (2019)
38. M.A.A. Farsangi, F. Cottone, H. Sayyaadi et al., Energy harvesting from structural vibrations of magnetic shape memory alloys. Appl Phys Lett **110**(10), 103905 (2017)
39. M.W. Shafer, E. Garcia, The power and efficiency limits of piezoelectric energy harvesting. J Vib Acoust **136**(2), 021007 (2014)
40. S.A. Brown, C.L. Hom, M. Massuda, J.D. Pardey, K. Bridger, N. Shankar, S.R. Winzer, Electromechanical testing and modeling of a relaxor ferroelectric. Journal of the AmericanCeramic Society **79**(9), 2271–2282 (1996)
41. L.X. Wang, Y. Chen, W.L. Zhao, Macroscopic differential model for hysteresis and buttery-shaped behavior in ferroelectric materials. Advanced Materials Research **47–50**, 65–68 (2008)
42. L.X. Wang, R. Melnik, Control of coupled hysteretic dynamics of ferroelectric materials with a Landau-type differential model and feedback linearization. Smart Mater Struct **18**(7), 074011 (2009)
43. S.A. Brown, C.L. Hom, M. Massuda et al., Electromechanical Testing and Modeling of a Relaxor Ferroelectric. J Am Ceram Soc **79**(9), 2271–2282 (1996)
44. Wang L, Willatzen M. Modeling of nonlinear responses for reciprocal transducers involving polarization switching. IEEE Trans Ultrasonics Ferroelectr Freq Control 2006, 54(1): 177–189.
45. S. Patel, A. Chauhan, R. Vaish, A technique for giant mechanical energy harvesting using ferroelectric/antiferroelectric materials. J Appl Phys **115**(8), 084908 (2014)
46. Dong W. Characterization, Modeling, and Energy Harvesting of Phase Transformations in Ferroelectric Materials. UCLA, 2015.